



HAL
open science

Micro-scale investigation of the role of finer grains in the behavior of bidisperse granular materials

Habib Taha, Ngoc-Son Nguyen, Didier Marot, Abbas Hijazi, Khalil Abou-Saleh

► **To cite this version:**

Habib Taha, Ngoc-Son Nguyen, Didier Marot, Abbas Hijazi, Khalil Abou-Saleh. Micro-scale investigation of the role of finer grains in the behavior of bidisperse granular materials. *Granular Matter*, 2019, 21 (2), 10.1007/s10035-019-0867-9 . hal-02332421

HAL Id: hal-02332421

<https://hal.science/hal-02332421>

Submitted on 8 Oct 2023

HAL is a multi-disciplinary open access archive for the deposit and dissemination of scientific research documents, whether they are published or not. The documents may come from teaching and research institutions in France or abroad, or from public or private research centers.

L'archive ouverte pluridisciplinaire **HAL**, est destinée au dépôt et à la diffusion de documents scientifiques de niveau recherche, publiés ou non, émanant des établissements d'enseignement et de recherche français ou étrangers, des laboratoires publics ou privés.

Micro-mechanical behavior of gap graded granular materials: a numerical study using DEM

Habib Taha · Ngoc-Son Nguyen ·
Didier Marot · Abbas Hijazi · Khalil
Abou-Saleh

the date of receipt and acceptance should be inserted later

Abstract This paper presents a numerical study of the effect of fine content on the mechanical behavior of gap-graded granular materials using the discrete element method. Triaxial compression tests are performed on different samples with fine contents varied from 0% to 40%. It was found that, starting from 20%, fine content has a visible effect on the shear strength. The optimal fine content is about 30%, at which the shear strength is the best. An investigation into the granular micro-structure showed that the fine particles, on one hand, come into contact with coarse particles, but on the other hand, separate the latter ones as fine content increases beyond 20%. Consequently, the shear stress is transmitted more and more through the coarse-fine contacts but less and less through the coarse-coarse contacts. For fine content $\leq 30\%$, the coarse-coarse contacts primarily carry the shear stress. Above this optimal fine content, the fine-coarse contacts overtake the coarse-coarse ones. The fine-fine contacts have little contribution to supporting the shear stress. For the studied range of fine content, the coarse particles primarily carry the shear stress, leaving the fine particles under relatively low stresses. Moreover, the fine particles are greatly softened by the shear loading. A classification of binary mixtures depending on their micro-structure was also proposed.

Keywords Gap-graded materials · Discrete element method · Shear loading · Micro-structure · Stress transmission · Contact network

Habib Taha · Ngoc-Son Nguyen · Didier Marot
GeM Institute, University of Nantes, 58 rue Michel Ange, BP 420, 44606, Saint-Nazaire
Cedex, France

Habib Taha · Abbas Hijazi · Khalil Abou-Saleh
MPLAB-Multidisciplinary Physics Laboratory, Faculty of Sciences, Lebanese University,
Hadat-Baabda, Lebanon

1 Introduction

Granular materials are often used for construction of hydraulic earth structures such as dikes, levees, dams, etc. Under the action of the fluid flow, a soil with gap-graded particle-size distribution (PSD) or widely graded and upwardly concave PSD are susceptible to internal erosion, during which fine particles can be detached and transported by seepage forces through the pore space between coarse particles [1]. The migration of fine particles in the soil modifies its porosity and its micro-structure. As a consequence, internal erosion could reduce the shear strength of the soil [2,3], hence the stability of hydraulic earth structures. The mechanical consequence of internal erosion is still an open research topic. It requires a deep understanding of the contribution of fine particles to the mechanical behavior of these soils.

The role of fine particles on the drained and undrained stress-strain behaviors of silty sands have been experimentally investigated by several authors [4–7]. Salgado et al. [4] observed that the drained shear strength and the dilatancy of silty sands increase with silt content. Thevanayagam et al. [5] investigated the effect of fine content on the undrained collapse potential, which is defined as the ratio of the maximum pore pressure induced by the shear to the confining pressure. The authors found a threshold value for fine content, under which the collapse potential increases with fine content but above which it decreases with fine content. The authors attributed these opposite effects of fine content to a variation of the granular micro-structure. They made a conjecture that, with increasing fine content, the micro-structure of granular mixtures can change from a category where contacts between coarse grains are dominant to a category where contacts between fine grains are dominant. This conjecture should be verified by investigating experimentally the granular micro-structure. Such an investigation might be performed by using X-ray tomography imaging technology [8], however, this technique is quite delicate and expensive. To the best of our knowledge, no experimental investigation of the effect of fine content on the granular micro-structure has been performed so far.

Discrete Element Method (DEM) has been widely used to simulate numerically granular media. This method was found to be able to reproduce the main features of the mechanical behavior of granular materials such as the non-linearity, the softening phase, the dilatancy and the induced anisotropy [9]. One of its main advantages is that any local information at the particle scale can be accessed, which make the DEM very suitable for investigating granular media from a micro-mechanical point of view. This method has been recently used by some authors to investigate the micro-structure and the micro-mechanical behavior of granular mixtures. Minh et al. [10,11] studied the contact force distribution and the force networks in granular mixtures under one-dimensional compression. Shire et al. [12,13] investigated the micro-structure and micro-properties of granular mixtures under isotropic compression. It is worth mentioning that a granular material subjected to a one-dimensional or an isotropic compression shows only a contractive behavior and never reaches the failure.

Tang-Tat et al. [14] studied the effect of particle shape and fine content on the behavior of binary mixtures using the DEM. The authors simulated triaxial compression tests on binary mixtures of ellipsoids with few numbers of coarse particles (25, 56 and 150 for $f_c = 50\%$, 30% and 10% , respectively). These mixtures hardly fulfill, therefore, the conditions required for the representative volume element. In addition, the effect of fine content on the behavior of binary mixtures is not clear. It is not well understood yet how the fine particles affect the behavior of granular mixtures under shear loading, from a micro-mechanical point of view.

This paper presents a numerical study of the effect of fine content on the behavior of granular mixtures under shear loading. Triaxial compression tests are simulated on granular materials with gap-graded particle size distribution by using the DEM (Section 2). The effect of fine content on the behavior of granular mixtures is analyzed at the macro-scale (Section 3) as well as at the micro-scale (Section 4). Our micro-mechanical investigation focuses on (i) the role of fine particles in the granular micro-structure, (ii) the stress transmission through the contact network and the force networks in a granular mixture, and (iii) the contribution of fine particles in carrying the overburden stress.

2 Numerical simulation with the DEM

A dry cohesionless granular soil is an assembly of distinct particles which can be assumed to be rigid. The interaction between particles can only occur at frictional interfaces. The DEM models dry granular media as they are. This method has the two following main ingredients: (i) Newton-Euler dynamic equation to describe the translational and rotational motions of each rigid particle, and (ii) a contact law to calculate the interaction force at the contact between two particles. An explicit or implicit time-stepping scheme is used to numerically integrate the dynamic equation. At each step, the velocity and the position of each particle are integrated up to the end of the step. At the same moment, contacts between particles are detected and contact forces are calculated from the velocity and the position of particles in contact. There are two main approaches for the DEM, which differ from each other in the way of modeling the interaction at contact. The Molecular Dynamic (MD) approach considers a small compliance effect at the contact point so the contact force can be uniquely determined from the elastic relative displacement at the contact point [15]. On the other hand, the Contact Dynamic (CD) approach neglects the compliance effect at the contact point. As a consequence, the contact force cannot be uniquely determined from the relative displacement at the contact point without considering the dynamic equation of the whole system [16]. In both approaches, Coulomb's friction law is used in the tangential direction to limit the tangential force. For the MD approach, an explicit integration scheme of high order can be used with a time step sufficiently small to describe accurately the dynamic process at the contact point. For the CD approach,

the numerical integration can only be done implicitly, but with a time step much bigger than that used in the MD approach.

We use the DEM based on the MD approach, which is implemented in the open-source software YADE [17]. In this preliminary study, for the sake of simplicity, spherical particles are considered with a linear contact force-displacement model at each contact between two particles. According to this contact law, the normal and tangential interactions at a contact are modeled by two linear springs with respective stiffnesses K_n and K_t . The contact normal and tangential stiffnesses are calculated from the respective particle stiffnesses by assuming that the latter ones are connected in series in each direction:

$$K_n = \frac{k_n^i k_n^j}{k_n^i + k_n^j} \quad \text{and} \quad K_t = \frac{k_t^i k_t^j}{k_t^i + k_t^j}, \quad (1)$$

where superscripts i and j denote two particles at the contact point; and k_n and k_t are particle normal and tangential stiffnesses, respectively. The tangential force f_t is limited by Coulomb friction law: $|f_t| \leq f_n \tan \varphi$ where f_n is the normal force and φ is the friction angle. The microscopic parameters used in our simulations are identical to those used in the paper of Scholtès et al. [18]: normal particle stiffness $k_n/D = 250$ MPa with particle diameter D , stiffness ratio $k_t/k_n = 0.5$ and friction angle $\varphi = 35^\circ$.

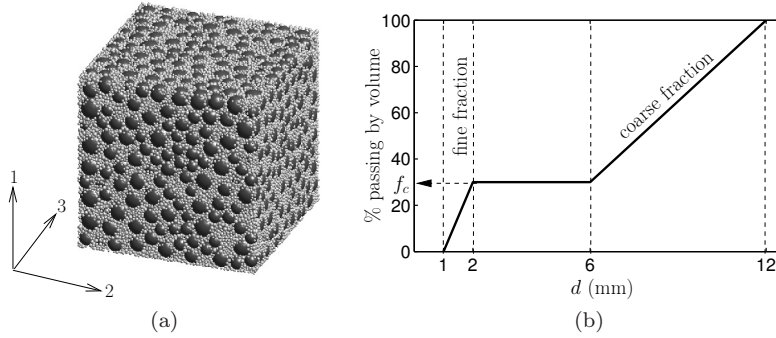


Fig. 1 (a) A simulated granular mixture and (b) the considered gap-graded grain size distribution.

Granular samples considered in this study are binary mixtures of coarse and fine particles (Figure 1.a). The particle size distribution (PSD) is a gap-graded curve as shown in Figure 1.b. This gap-graded PSD is characterized by fine content f_c and the gap ratio $G_r = D_{\min}/d_{\max}$ (D_{\min} is the minimum diameter of coarse particles and d_{\max} is the maximum diameter of fine particles). Fine content f_c is varied from 0% to 40%. A value of 3 is chosen for the gap ratio G_r to keep the computation time reasonable since a higher value of G_r leads to a large number of particles and then to a very long computation time. It is worth mentioning that, according to Chang and Zhang [19], a gap-graded soil

with gap ratio of 3 might be unstable – in other words, fine particles might migrate due to seepage flow.

Particles are first generated into a cube composed of six rigid walls. At this stage, each particle diameter is reduced by a factor of 2.0. Particles are then progressively expanded to reach the target size distribution. After that, the box dimensions are slowly reduced until the stresses σ_i ($i = 1, 2, 3$) reach the confining stress of 100 kPa. To obtain dense samples, the friction angle φ is set to 0° during the compaction process and then is reset to its original value (35°) at the end of the compaction process. Triaxial compression tests are then performed by prescribing a small strain rate $\dot{\epsilon}_1 = 0.01 \text{ s}^{-1}$ in direction (1), while keeping the lateral stresses σ_2 and σ_3 constant.

Table 1 Respective numbers, N_c and N_f , of coarse and fine particles, ratio L/D_{\max} and coefficient of dispersion C_v for different values of fine content f_c .

f_c	N_c	N_f	L/D_{\max}	C_v	f_c	N_c	N_f	L/D_{\max}
0%	1430	0	7.5	1.1%	25%	1 296	93170	7.3
5%	1347	15305	7.3	3.0%	30%	1 246	115186	7.4
10%	1266	30346	7.2	2.3%	35%	1 063	123 386	7.2
15%	1276	48571	7.2	1.6%	40%	982	141198	7.2
20%	1273	68646	7.2	1.7%				

Table 1 shows the number of coarse particles (N_c), the number of fine particles (N_f) and the ratio L/D_{\max} of the sample size to the maximum particle diameter for different values of fine content f_c . Since the number of fine particles increases quickly with fine content, the number of coarse particles is carefully chosen such that the total number of particles is not too large and the simulated samples can be considered as Representative Volume Elements

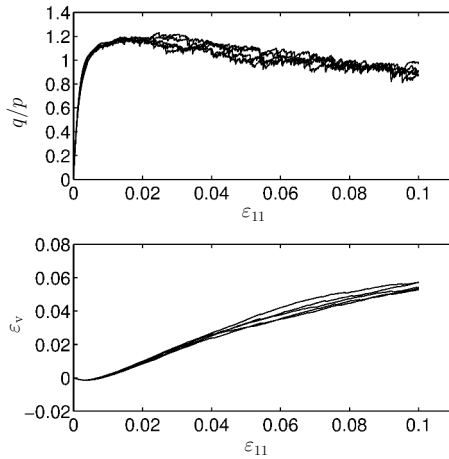


Fig. 2 Stress ratio q/p and volumetric strain ϵ_v versus axial strain ϵ_{11} for five different samples randomly generated with $f_c = 20\%$ with $L/D_{\max} = 7.2$.

(RVE). The choice of the sample size for a gap-graded PSD is not an easy task. One might rely on experimental norms for triaxial compression tests in laboratory. For example, the ASTM standard [20] recommended that the ratio of the specimen diameter to the largest particle size is larger than 6, while the French standard [21] recommended a value larger than 5 for widely graded soils and 10 for uniformly graded soils. It should be noted that the chosen sample sizes shown in Table 1 satisfy these criteria. For DEM numerical simulations, no clear rule has been established. Wiącek and Molenda [22] showed that for polydisperse granular packings which are not widely graded and are subjected to an uniaxial compression, the RVE size is about 15 times the average particle diameter, i.e. the sample must include at least $15 \times 15 \times 15 = 3375$ particles. Sallot et al. [23] found out that the RVE size for simulating a triaxial compression test on samples having a tight and uniform PSD is about 8000 particles. For a gap-graded PSD, the number of particles should be varied with fine content, and 8000 particles are, in general, not enough. Shire et al. [24] have stated that a gap-graded sample with a minimum of 500 coarse particles can be considered as a RVE when simulating an isotropic compression. A shear loading might require a larger number of coarse particles to achieve a RVE. It is worth noting that the RVE size for a granular material is determined in a statistical sense. This means that different random generations of samples with the same size must give close results as stated by Chareyre [25]. We have adopted this statistical approach to check the RVE for the simulated binary mixtures under shear loading. For a given value of fine content f_c with the chosen sample size, five samples are randomly generated, compacted and then subjected to triaxial compression tests in the same manner. Figure 2 shows the ratio q/p of the deviatoric stress $q = \sigma_{11} - \sigma_{33}$ to the mean stress $p = (\sigma_{11} + 2\sigma_{33})/3$ and the volumetric strain ε_v versus the axial strain ε_{11} for five different samples randomly generated for $f_c = 20\%$ with the chosen sample size $L/D_{\max} = 7.2$. It can be seen that these five random samples with the same size give close behaviors. The dispersion in terms of shear strength (maximum value of the stress ratio q/p) is characterized by the coefficient of variation C_v used in the statistical analysis. The values of C_v for $f_c = 0\%, 5\%, 10\%$ and 20% are shown in Table 1. These low values of C_v indicate that the chosen sample sizes for $f_c = 0, 5, 10, 15$ and 20% can be considered as RVE sizes. For $f_c \geq 25\%$, we did not perform this repeatability study because the simulation of samples with a high fine content is very time-consuming. However, the samples with $f_c = 25\%$ and 30% can be considered as RVEs as they contain almost the same number of coarse particles as the sample with $f_c = 20\%$. For the samples with $f_c = 35\%$ and 40% , the number of coarse particles is reduced to gain the computational time while maintaining almost the same sample size. With around 1000 coarse particles, compared to the value of 500 indicated in [24], these samples can be expected to be RVEs. It is worth mentioning that the number of particles used for $f_c = 0\%$ is smaller than 8000 particles recommended in [23]. However, the dense state of the generated samples reduces significantly the dispersion of their behavior.

3 Macroscopic investigation

3.1 Void ratios

In a mixed soil that contains a fine content smaller than a threshold value, coarse particles may constitute a solid skeleton to carry mainly the overburden stress. A significant fraction of fine particles may be confined within pores between the former ones and then they may not participate in sustaining the shear stress as assumed by several authors [26,27]. According to Thevanayagam and Mohan [27], the global void ratio, e , defined as the ratio of the volume of actual voids to the volume of solids may not adequate to describe the density of such a mixture. The authors proposed to consider a mixed soil as a composite medium consisting of two matrices: coarse-grained matrix and fine-grained matrix. The intergranular void ratio, e_c , and interfine void ratio, e_f , were then introduced to describe the density of the coarse-grained and fine-grained matrices, respectively. The intergranular void ratio e_c is defined by assuming that all fine particles do not sustain any stress and can be considered as the intercoarse voids. On the other hand, the interfine void ratio e_f is defined by considering that the coarse particles are of zero volume.

$$e_c = \frac{V_v + V_s^F}{V_s^C} = \frac{e + f_c}{1 - f_c}, \quad e_f = \frac{V_v}{V_s^F} = \frac{e}{f_c}, \quad (2)$$

where V_v , V_s^F and V_s^C are the void volume and the total solid volumes of the fine particles and of the coarse particles, respectively.

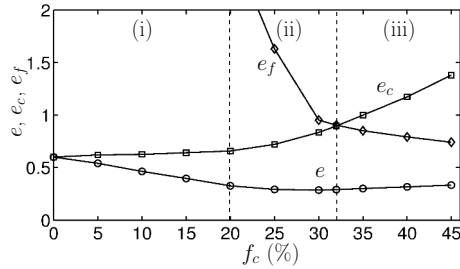


Fig. 3 Global void ratio e , intergranular void ratio e_c and interfine void ratio e_f versus fine content f_c .

Figure 3 presents the three void ratios e , e_c and e_f versus fine content f_c for the simulated samples. Three remarkable ranges of fine content with two threshold fine contents $f_c = 20\%$ and $f_c = 32\%$ can be identified. For the range (i) with $f_c < 20\%$, the intergranular void ratio e_c remains more or less constant, while the interfine void ratio e_f decreases quickly with increasing fine content f_c . This means that the fine particles fill voids left by the coarse particles without separating the latter ones. As a result, the global void ratio e decreases

as fine content increases. It is worth mentioning that the interfine void ratio e_f for this range of fine content is very high compared to the intergranular void ratio e_c and the curve for e_f cannot be fully represented in the chosen scale in Figure 3. Within the range (ii) with $20\% \leq f_c < 32\%$, the fine particles separate the coarse ones and occupy the void space between them. The fine-grained matrix gets denser but the coarse-grained matrix gets looser. It should be noted that, for this range of fine content, the coarse-grained matrix is still denser than the fine-grained matrix. One would expect that there exists an intermediate configuration where all fine particles fill fully voids between coarse particles without separating them; however, this is not the case. As shown in Figure 3, at $f_c = 20\%$, fine particles begin to intercalate between coarse ones but the interfine void ratio e_f is still very large. This means that intercoarse voids are not fully filled yet by the fine particles. It is interesting to note that, at the last threshold fine content $f_c = 32\%$, the interfine void ratio e_f is equal to the intergranular one e_c , and the global void ratio e reaches its minimum value. Lade et al. [28] also observed an optimal fine content at which the global void ratio is minimum when analyzing experimentally the density of mixtures of coarse and fine spherical balls. In these experiments, coarse balls of the same diameter D are mixed with fine balls of the same diameter d . The coarse balls are deposited first in a container and the fine balls are then added from the top while the container is vibrated. For mixtures with the ratio $D/d = 3.5$, the optimal fine content is about 40%. It should be noted that the difference between the optimal fine content of 32% found in our study and the value of 40% shown in [28] may be related to the fact that the coarse balls, as well as the fine balls, are of different size and they are generated and compacted simultaneously in our study. In doing so, the fine balls have more chance to be intercalated between the coarse particles. For the range (iii) where fine content goes beyond 32%, the coarse particles are greatly separated by the fine ones and the coarse-grained matrix gets looser than the fine-grained matrix.

3.2 Stress-strain behavior

Figure 4 shows the stress ratio q/p and the volumetric strain ε_v versus the axial strain ε_{11} for the simulated samples. The maximum and residual stress ratios q/p for different values of f_c are given in Table 2. It is found that the stress-strain behavior of the granular mixtures with $f_c < 20\%$ is not significantly affected by fine content (Figure 4.a). Starting from $f_c = 20\%$, fine content has opposite effects on the shear strength and dilatancy of the binary mixtures. The shear strength at the peak state increases with fine content $f_c \leq 32\%$ but decreases when $f_c > 32\%$ (Figure 4.b). It is interesting to note that the threshold fine content of 32% found here is also the threshold value observed in Figure 3 at which the intergranular and interfine void ratios are equal and the global void ratio is minimum. The same tendency is observed for the material dilatancy except that the threshold fine content for it is about 35%, which is also quite close to the value of 32% observed for the maximum shear strength.

As the stress-strain curve for $f_c = 32\%$ is almost coincident with the one for $f_c = 30\%$, we consider that the second fine content threshold is 30% instead of 32% and we do not show the results obtained with $f_c = 32\%$ in the following.

The above result means that a reasonable fine content ($20\% \leq f_c \leq 30\%$) can make granular materials stronger and more dilatant. This is in good agreement with experimental results of Salgado et al. [4] who performed drained triaxial tests on mixtures of clean Ottawa sand and silt. However, in this study, the role of fine particles was clearly observed even at a low fine content ($f_c \leq 15\%$). This might be explained by the fact that the sand-silt mixtures considered in their study have continuous and broadly graded PSDs, for which fine particles might fill the space between coarse particles even at low fine content. Figure 4.b also shows that a too high fine content ($f_c > 30\%$) can be a factor unfavorable to the shear strength and dilatancy of granular mixtures. The mixture with $f_c = 40\%$ has indeed a lower shear strength and a lower dilatancy than the mixture with $f_c = 30\%$. Thevanayagam et al. [5] also found that an important quantity of silica fines in sands reduces significantly their undrained shear strength.

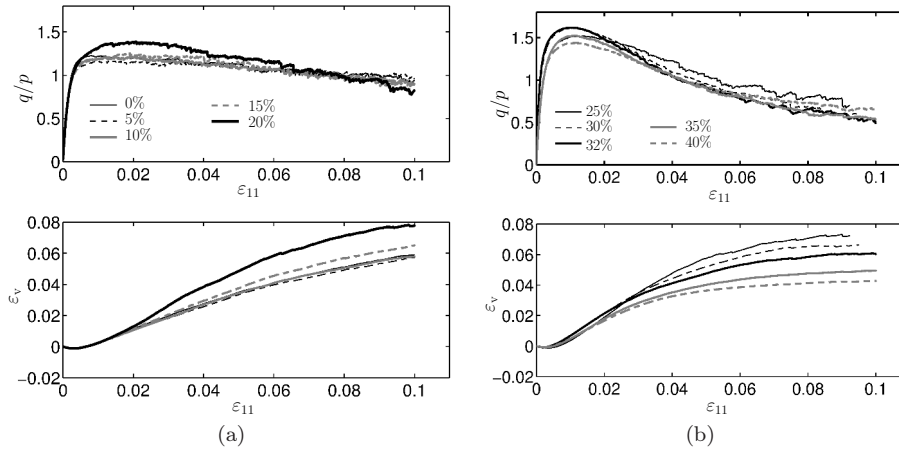


Fig. 4 Stress ratio q/p and volumetric stress ϵ_v versus axial strain ϵ_{11} for different values of fine content: (a) f_c varies from 0% to 20% and (b) f_c varies from 25% to 40%.

Table 2 Maximum and residual stress ratios $(q/p)_{\max}$ and $(q/p)_{\text{residual}}$ for different values of fine contents f_c .

f_c (%)	0	5	10	15	20	25	30	32	35	40
$(q/p)_{\max}$	1.1	1.1	1.2	1.2	1.3	1.5	1.6	1.6	1.5	1.4
$(q/p)_{\text{residual}}$	0.9	0.9	1.0	0.9	0.8	0.7	0.6	0.5	0.5	0.6

A dense granular sample exhibits a peak on the stress-strain curve, followed by a marked softening phase. This kind of behavior can be observed for the mixtures with $f_c \geq 20\%$. The critical state is an important concept in soils mechanics, at which soils deform without any change in their volumetric strain and their shear strength. Soils reach, in general, this particular state at large strain (around 30%). As shown in Figure 4, all the simulated samples do not reach the critical state yet. However, at the axial strain $\varepsilon_{11} = 10\%$, the stress ratio q/p remains more or less constant so we assume that the critical state is almost reached at this value of the axial strain. It is interesting to note in Figure 4.b that fine particles, on one hand, strengthen granular mixtures at the peak state, but on the other hand, weaken them at the critical state. The stress ratio q/p for $f_c = 30\%$ is 1.6 at the peak state and 0.6 at the critical state, compared to the respective values 1.1 and 0.9 for $f_c = 0\%$.

One could try to explain the effect of fine content on the mechanical behavior of granular mixtures by using the dependency of the void ratios e , e_c and e_f upon fine content f_c shown in Figure 3. The negligible effect of fine particles on the stress-strain behavior observed for the mixtures with $f_c < 20\%$ is related to the fact that the fine fraction is very loose (range (i) in Figure 3) so the fine particles do not participate actively in supporting the external loading. However, it is not easy to explain why the shear strength and the dilatancy increase with fine content when $f_c > 20\%$ but decrease when $f_c > 30\%$, and why a mixture with a significant fine content shows a marked softening phase. It should be noted that adding fine particles into a mixture leads to two opposing effects: on one hand, the coarse fraction gets looser, which weakens the mixture, but on the other hand, the fine fraction gets denser, which strengthens the mixture. It is not well understood yet which effect is more important than the other for a given fine content. In the following, we bring some insights into granular mixtures to have a better understanding of how fine particles modify the granular micro-structure and participate in sustaining the applied shear stress.

4 Microscopic investigation

4.1 Coordination numbers

Coordination number, denoted by \mathcal{N} , is defined as the average number of contacts per particle. It is usually used to describe the density of a granular assembly at the micro-scale. However, this definition of the coordination number is not appropriate for a mixture of coarse and fine particles because the number of contacts per coarse particle is very different from that per fine particle. As mentioned previously, a binary granular mixture can be thought of being a multi-phase medium which is composed of the coarse-grained matrix, the fine-grained matrix and the interface between them. The interaction between particles in each phase occurs through $C - C$ contacts (between two coarse particles), $F - F$ contacts (between two fine particles), respectively;

and these two phases interact each other through $C - F$ contacts (between a coarse and a fine particle). Describing the local density of the coarse-grained and fine-grained matrices and the interface between them needs thus three coordination numbers, denoted by \mathcal{N}_C^{C-C} , \mathcal{N}_F^{F-F} and \mathcal{N}_C^{C-F} , which are defined as the respective average numbers of $C - C$ contacts per coarse particle, of $F - F$ contacts per fine particle, and of $C - F$ contacts per coarse particle. Minh and Cheng [29] and Shire et al. [13,30] also defined similar coordination numbers to study the micro-structure of granular mixtures.

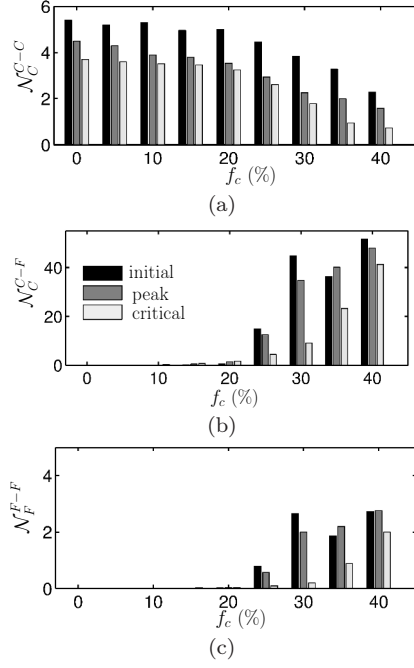


Fig. 5 Coordination numbers (a) \mathcal{N}_C^{C-C} , (b) \mathcal{N}_C^{C-F} and (c) \mathcal{N}_F^{F-F} versus fine content f_c at the initial, peak and critical states.

Figures 5.a, 5.b and 5.c show the respective coordination numbers \mathcal{N}_C^{C-C} , \mathcal{N}_C^{C-F} and \mathcal{N}_F^{F-F} versus fine content f_c at the initial, peak and critical states. It can be seen that, at the initial state, the coordination number \mathcal{N}_C^{C-C} remains more or less constant and the coordination numbers \mathcal{N}_F^{F-F} and \mathcal{N}_C^{C-F} are very small for $f_c < 20\%$. This confirms the statement made in Section 3.1 that the fine particles are almost floating within voids between coarse ones and they do not modify the granular skeleton which is mainly constituted of coarse particles. Starting from $f_c = 20\%$, a further addition of fine particles leads, on the whole, to a strong increase in \mathcal{N}_C^{C-F} and \mathcal{N}_F^{F-F} , particularly for \mathcal{N}_C^{C-F} , but to a remarkable decrease in \mathcal{N}_C^{C-C} . This means that the presence of an important fine content in a granular material induces two opposing effects.

On one hand, fine particles disrupt contacts between coarse ones and then weaken the coarse fraction. On the other hand, a significant quantity of fine particles around each coarse particle reinforce the interface between the coarse-grained and fine-grained matrices. Furthermore, more contacts between fine particles are created, allowing the shear stress to be transmitted through the fine-grained matrix as will be shown in the next section. Shire et al. [30] also observed a decrease in number of contacts per coarse particle and an increase in number of contacts per fine particle with increasing fine content on granular mixtures with bigger values of the gap ratio G_r . The best shear strength at the peak state for $f_c = 30\%$ shown in Figure 4.b can be attributed to the fact that the coarse particles are strongly reinforced by an important number of fine particles around them (about 50 fine particles, on average), despite the fact that they are slightly weakened by a loss of contacts between them.

Figure 5 also shows a remarkable decrease in the coordination numbers \mathcal{N}_C^{C-C} , \mathcal{N}_C^{C-F} and \mathcal{N}_F^{F-F} at the peak and critical states for the samples with $f_c > 20\%$. The most drastic drop in \mathcal{N}_C^{C-C} , \mathcal{N}_C^{C-F} and \mathcal{N}_F^{F-F} is observed for $f_c = 30\%$: \mathcal{N}_C^{C-C} and \mathcal{N}_C^{C-F} decrease from 3.8 and 44.9 at the initial state to 1.8 and 9.1 at the critical state, respectively. This drastic drop in the coordination numbers means that the micro-structure of the samples with $f_c > 20\%$ is strongly altered after the peak state.

The next section gives us more insights into how the shear stress is transmitted through the coarse-coarse, coarse-fine and fine-fine contacts in granular mixtures.

4.2 Stress transmission through the contact network

When a granular sample is subjected to an external loading, contacts between particles participate in transferring forces [31,32]. The stress tensor defined at the macro-scale can be related to contact forces at the micro-scale by using the following static homogenization operator [33]:

$$\sigma_{ij} = \frac{1}{V} \sum_k f_i^k l_j^k. \quad (3)$$

The stress tensor σ is defined on a volume V whose boundary is tangent to the particles that are close to it (Figure 6). Superscript k runs over not only all contacts between particles (interior contacts) but also all contacts between particles and the boundary. For a contact between two particles, \mathbf{f}^k is the contact force and \mathbf{l}^k is the branch vector joining two particle centers at this contact. For a contact between a particle and the boundary, \mathbf{f}^k is the force exerted by the exterior to the particle and the vector \mathbf{l}^k joins the particle center to the contact point.

It has been well known in the literature that the static homogenization operator (3) gives a good estimation of the macroscopic stress tensor if the volume under consideration contains a sufficient number of particles. This can be confirmed in Figure 7 where the mean stress p estimated with (3) is

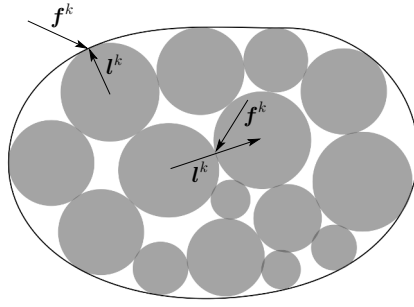


Fig. 6 Illustration of a volume on which the stress tensor σ is defined.

compared to the value of 100 kPa applied on the boundary at the initial state for different values of fine content f_c . Figure 7 also shows that the contribution of the contacts between particles and the boundary (the rigid walls in our simulations) to the macroscopic stress tensor σ is not negligible (about 10% for $f_c \leq 20\%$) and it decreases as fine content f_c increases (about 4.5% for $f_c = 40\%$). This is due to the fact that the sample sizes L chosen for the simulated samples (Table 1) are not too large compared to the maximum particle size D_{\max} so the number of contacts on the boundary is not negligible compared to the number of interior contacts. It is expected that the stress part relative to the contacts on the boundary is negligible compared to that relative to the interior contacts when the sample size is big enough compared to the particle size. The contacts on the boundary result indeed in no more than 2% of the macro-stress for a sample of $f_c = 0\%$ with $L/D_{\max} = 38$.

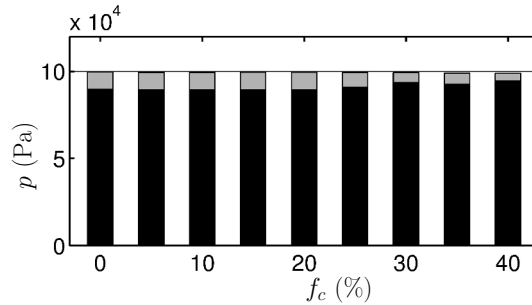


Fig. 7 The mean stress p estimated with (3) at the initial state is compared to the mean stress $p = 100$ kPa applied on the boundary of samples with different values of fine content f_c . Black and gray colors represent the contributions of the interior contacts and of the contacts on the boundary, respectively

The stress part relative to the contacts between particles can be split into three parts σ^{C-C} , σ^{C-F} and σ^{F-F} which correspond to the contributions of

the respective categories of $C-C$, $C-F$ and $F-F$ contacts. For example, the contribution of the set of $C-C$ contacts to the stress tensor $\boldsymbol{\sigma}$ is computed as:

$$\sigma_{ij}^{C-C} = \frac{1}{V} \sum_{k \in C-C} f_i^k l_j^k. \quad (4)$$

The stress tensors $\boldsymbol{\sigma}^{C-C}$, $\boldsymbol{\sigma}^{C-F}$ and $\boldsymbol{\sigma}^{F-F}$ have the same principal directions as those of the macro-stress tensor $\boldsymbol{\sigma}$. The contributions of each category of contacts to the macroscopic mean and deviatoric stresses, p and q , can be calculated, for example $p^{C-C} = (\sigma_{11}^{C-C} + 2\sigma_{33}^{C-C})/3$ and $q^{C-C} = \sigma_{11}^{C-C} - \sigma_{33}^{C-C}$.

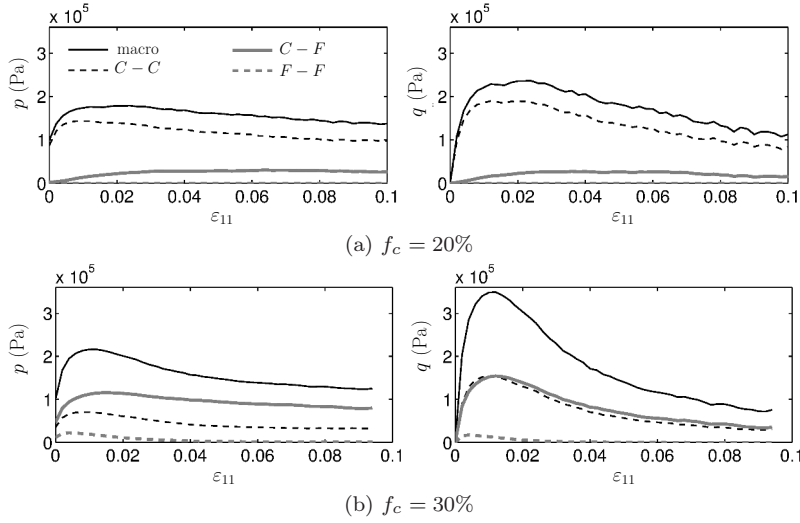


Fig. 8 Contribution of the three categories of $C-C$, $C-F$ and $F-F$ contacts to the macroscopic mean and deviatoric stresses, p and q , versus axial strain ε_{11} for (a) $f_c = 20\%$ and (b) $f_c = 30\%$.

The mean and deviatoric stresses calculated for the three categories of $C-C$, $C-F$ and $F-F$ contacts are plotted versus the axial strain ε_{11} in Figures 8.a and 8.b for $f_c = 20\%$ and $f_c = 30\%$, respectively. Their values at the peak and critical states are plotted versus fine content f_c in Figure 9. It is shown that, for $f_c < 20\%$, the $C-F$ and $F-F$ contacts do not contribute significantly to the macro-stress. For instance, for $f_c = 15\%$, all the $C-F$ contacts contribute to only 4% of the macroscopic mean and deviatoric stresses at the peak state. A major part of the macro-stress is carried by the $C-C$ contacts and it remains more or less constant for $f_c < 20\%$. This is in agreement with the result shown in Figure 5 where the coordination numbers \mathcal{N}_C^{C-F} and \mathcal{N}_F^{F-F} are negligible compared to \mathcal{N}_C^{C-C} which is not affected by a low fine content. Starting from $f_c = 20\%$, the $C-F$ contacts contribute

to supporting the shear stress. For this threshold value, the $C - F$ contacts carry about 10% of the macro-stress despite a low value of \mathcal{N}_C^{C-F} , while the stress part carried by the $C - C$ contacts is almost the same as that for the samples with $f_c < 20\%$ (Figures 8.a and 9). This explains why the effect of fine content on the shear strength is visible starting from 20% (Figure 4). It is worth mentioning that it is not easy to explain this if we look only at the void ratios in Figure 3 and at the coordination numbers in Figure 5.

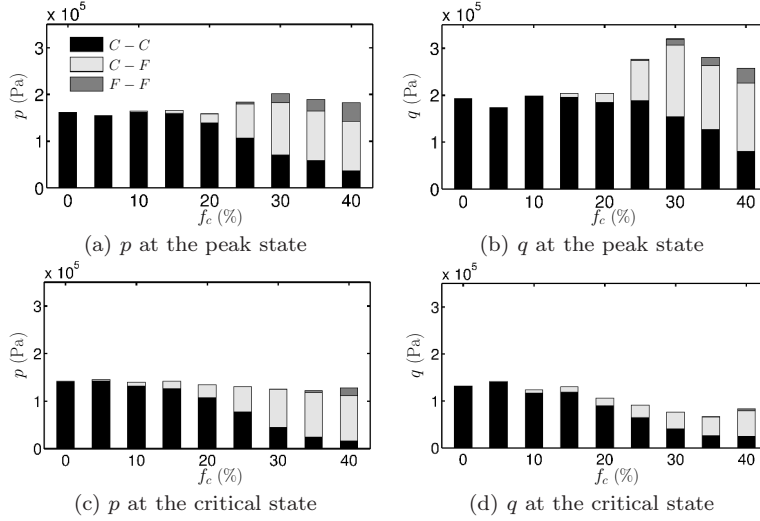


Fig. 9 Contributions of the three categories of $C - C$, $C - F$ and $F - F$ contacts to the macroscopic mean and deviatoric stresses, p and q , versus fine content f_c : (a) and (b) at the peak state and (c) and (d) at the critical state.

The $C - F$ and $F - F$ contacts participate more and more in sharing the macro-stress as f_c increases from 20% as shown in Figure 9. At $f_c = 30\%$, the $C - F$ contacts actually contribute to the deviatoric stress q as much as the $C - C$ contacts. Interestingly, they contribute even more to the mean stress p than the latter ones (see also Figure 8.b). The role of the $C - F$ contacts becomes more important than the role of the $C - C$ contacts at $f_c = 40\%$ at which the former ones contribute to about 53% of the deviatoric stress q at the peak state, compared to a value of 35% for the latter ones. The $F - F$ contacts have a visible contribution to the macro-stress at the peak state when $f_c \geq 30\%$; however, their contribution is quite small, compared to those of the $C - C$ and $C - F$ contacts. At $f_c = 40\%$, the $F - F$ contacts contribute to 22% of the mean stress p and to 12% of the deviatoric stress q . The increasing role of the $C - F$ and $F - F$ contacts and the decreasing role of the $C - C$ contacts with increasing fine content from 20% are related to the increase in the coordination numbers \mathcal{N}_C^{C-F} and \mathcal{N}_F^{F-F} , and to the decrease in the coordination number \mathcal{N}_C^{C-C} (Figure 5), respectively. One can remark that the $C - C$ and $C - F$

contacts reverse their roles in sustaining the shear stress at the threshold fine content of 30%: above this value, the latter ones sustain more the shear stress than the former ones. The contribution of the $C - F$ contacts to the macro-stress increases quickly with $f_c \leq 30\%$, which compensates a decrease in the contribution of the $C - C$ contacts. As a consequence, the shear strength at the peak state increases with fine content $f_c \leq 30\%$. However, an increase in fine content f_c from 30% does not lead to a significant increase in the stress part carried by the $C - F$ contacts but leads to a strong decrease in the stress part carried by the $C - C$ contacts. Consequently, the shear strength at the peak state decreases with fine content $f_c > 30\%$. It can be expected that, at a very high fine content, the coarse particles are fully dispersed by the fine particles. In this case, the shear stress is mainly carried by the $C - F$ and $F - F$ contacts.

Figure 9 also shows a marked decrease in the deviatoric stresses supported by the three categories of contacts at the critical state for the samples with $f_c \geq 30\%$. The most drastic drop is observed for the sample with 30% of fine content where the deviatoric stresses supported by the $C - C$ and $C - F$ contacts are reduced by a factor > 3 from the peak state to the critical state. As a consequence, its shear strength is greatly reduced at the critical state, which is consistent with the great degradation of its micro-structure after the peak state as shown in Figure 5. The deviatoric stress carried by the $C - C$ contacts for the sample with $f_c = 30\%$ becomes much lower than that for the sample with $f_c = 0\%$ at the critical state. In addition, the $C - F$ contacts in the former sample suffer a great softening phase. This explains why the residual shear strength for $f_c = 30\%$ is lower than that for $f_c = 0\%$ (Table 2). It is interesting to note in Figure 9 that the mean stress at the critical state is primarily carried by the $C - F$ contacts for $f_c \geq 30\%$, and the $F - F$ contacts carry almost no stress at this state.

We have shown in this section that the external stress applied to a binary mixture is mainly transmitted through the $C - C$ and $C - F$ contacts. It does not mean that all the $C - C$ or $C - F$ contacts carry in the same manner the external stress since force transmission through a granular medium is well known to be very heterogeneous. In the same system, there exist strong and weak force networks with different roles in sustaining the shear stress. In the next section, we analyze how the contacts in each category constitute the strong and weak force networks.

4.3 Strong and weak force networks

According to the definition of Radjai et al. [32], the weak and strong force networks are composed of the contacts where the contact force f^c is smaller and bigger than the average contact force \bar{f} , respectively. The authors found that the strong network sustains almost the shear stress and the weak network behaves like a liquid without bearing any shear stress. The same result is obtained for the binary mixtures considered in this study as shown in Figure

10. It can be seen that the weak network sustains a small part of the mean stress p but a negligible part of the deviatoric stress q .

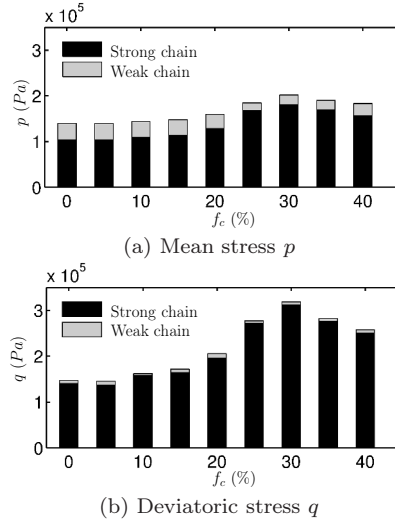


Fig. 10 Contributions of the strong and weak force chains to the mean stress p and the deviatoric stress q versus fine content f_c .

Figure 11 shows the fraction of $C - C$, $C - F$ and $F - F$ contacts in the strong network for the considered binary mixtures at the peak state. For each category, the fraction of contacts in the strong force network is defined as the ratio of the number of its contacts in the strong force network to the total number of its contacts. It can be seen that, at low fine content ($f_c < 20\%$), the strong force network is constituted of about 40% of $C - C$ contacts and a much smaller fraction of $C - F$ contacts. As fine content increases, more $C - C$ contacts participate in the strong force network. More than 95% of $C - C$ contacts actually take part in the strong force network for $f_c \geq 30\%$. This can be explained by the fact that the presence of fine particles around coarse ones makes contacts between coarse particles stronger so they carry a much bigger force. It does not mean, however, that the $C - C$ contacts can carry a bigger stress: they carry, indeed, a lower stress at $f_c = 30\%$ than at $f_c = 10\%$ (Figure 9) because more $C - C$ contacts are disrupted by fine particles at $f_c = 30\%$. Figure 11 also shows that an increasing fraction of $C - F$ and $F - F$ contacts take part in the strong force network as fine content increases so they sustain more the shear stress. However, a major fraction of these contacts are located in the weak force network (more than 56% of $C - F$ contacts and 80% of $F - F$ contacts).

The above analyzes have shown how the macroscopic stress is transmitted through the contact network in a granular mixture but they do not show how much stresses the coarse and fine fractions carry. According to Skempton and

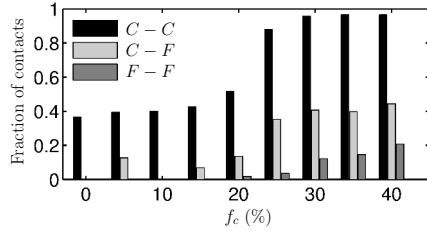


Fig. 11 Fraction of $C - C$, $C - F$ and $F - F$ contacts in the strong network at the peak state.

Brogan [26], the stress carried by the fine fraction is an important factor that influences the susceptibility of a granular material to internal erosion. In the next section, we define first the stresses carried by the coarse and fine fractions, and then we show how they depend on fine content.

4.4 Stresses carried by the fine and coarse fractions

In addition to the coarse-grained matrix (C) and the fine-grained matrix (F) in a granular mixture, voids (V), which can be filled by water or not, are present between solid particles. By homogenizing the stress field in this heterogeneous medium, the macroscopic stress can be defined from its counterpart within each phase:

$$\sigma_{ij} = \sum_{\alpha \in \{F, C, V\}} \phi^\alpha \sigma_{ij}^\alpha = \sum_{\alpha \in \{F, C, V\}} \hat{\sigma}_{ij}^\alpha. \quad (5)$$

For each phase α , ϕ^α is its volume fraction, i.e. the ratio of its volume V^α to the total volume V . The *intrinsic averaged stress* σ^α is defined as the average of the microscopic stress field $\sigma(\mathbf{x})$ which prevails in the phase under consideration:

$$\sigma_{ij}^\alpha = \frac{1}{V^\alpha} \int_{\mathbf{x} \in V^\alpha} \sigma_{ij}(\mathbf{x}) dV. \quad (6)$$

According to the mixture theory, the tensor $\hat{\sigma}^\alpha = \phi^\alpha \sigma^\alpha$ is called *partial stress*, which can be understood as the contribution of the phase under consideration to the macroscopic stress σ . It should be noted that it is the intrinsic averaged stress σ^α that gives information on how much the phase under consideration is stressed. For a dry mixture, voids bear zero-stress so we obtain:

$$\sigma_{ij} = \phi^F \sigma_{ij}^F + \phi^C \sigma_{ij}^C = (1 - n)[f_c \sigma_{ij}^F + (1 - f_c) \sigma_{ij}^C]. \quad (7)$$

The volume fraction ϕ^F of the fine fraction is related to fine content f_c and the porosity n by $\phi^F = (1 - n)f_c$.

Using the definition (6) with some transformations, one can define the intrinsic averaged stresses $\boldsymbol{\sigma}^F$ and $\boldsymbol{\sigma}^C$ in the fine and coarse fractions as follows:

$$\sigma_{ij}^F = \frac{1}{V_s^F} \sum_{p \in F} M_{ij}^p, \quad \sigma_{ij}^C = \frac{1}{V_s^C} \sum_{p \in C} M_{ij}^p, \quad (8)$$

where superscript p runs over all the particles in each fraction; and V_s^F and V_s^C are the respective total solid volumes of the fine particles and of the coarse particles. The tensor \mathbf{M}^p , called *internal moment tensor* by Moreau [34], is defined for each particle p as follows:

$$M_{ij}^p = \sum_{k \in p} f_i^k r_j^k \quad (9)$$

where the superscript k denotes each contact on the particle under consideration; the vector \mathbf{r}^k connects the particle center to the contact point; and \mathbf{f}^k is the contact force. As stated in [34,35], the physical meaning of the internal moment tensor \mathbf{M}^p remains the same when it is applied to a single particle or when it is applied to a collection of particles. Moreover, when it is applied to a large scale, i.e. a collection contains a large number of particles, its physical meaning tends to that of the Cauchy stress tensor. It should be noted that the estimated macroscopic stress tensor defined by (3) can be recovered by summing the tensors \mathbf{M}^p over all the particles:

$$\sigma_{ij} = \frac{1}{V} \sum_p M_{ij}^p. \quad (10)$$

The definition (8) can also be transformed to

$$\sigma_{ij}^F = \frac{1}{V_s^F} \sum_{p \in F} \sigma_{ij}^p V_s^p, \quad \sigma_{ij}^C = \frac{1}{V_s^C} \sum_{p \in C} \sigma_{ij}^p V_s^p, \quad (11)$$

where $\boldsymbol{\sigma}^p$ is the stress tensor defined for each particle with the solid volume V_s^p : $\boldsymbol{\sigma}^p = \mathbf{M}^p / V_s^p$.

Inspired from the stress reduction factor α for the fine fraction that was introduced by Skempton and Brogan [26], we define two stress factors α_p^F and α_q^F , which are the ratios of the mean and deviatoric stresses carried by the fine fraction, p^F and q^F , to their macroscopic counterparts, p and q , respectively

$$\alpha_p^F = p^F / p, \quad \text{and} \quad \alpha_q^F = q^F / q, \quad (12)$$

where p^F and q^F are computed from the intrinsic averaged stress tensor $\boldsymbol{\sigma}^F$ defined by (8). The defined stress factors α_p^F and α_q^F can be thought of as being the relative mean and deviatoric stresses carried by the fine fraction, compared to the macroscopic counterparts. It is worth mentioning that if both fractions carried the same stress, these two stress factors would be $\alpha_p^F = \alpha_q^F = 1/(1-n)$. Shire et al. [24] defined a stress reduction factor $\alpha = p^F / p$ for the fine fraction. The authors computed the averaged stress $\boldsymbol{\sigma}^F$ in the fine fraction using the

definition (11). However, instead of considering the solid volume V_s^p of each particle, the authors associated to each particle an amount of void surrounding it, so the volume considered for each particle when computing the averaged stress σ^p is $V^p = V_s^p/(1-n)$. By doing so, a binary mixture is considered as a biphasic material: fine and coarse fractions with the respective total volumes $V^F = V_s^F/(1-n)$ and $V^C = V_s^C/(1-n)$; and the resulting stress σ^F is no longer intrinsic to the solid fraction of the fine particles according to (6).

Figure 12 shows the absolute mean and deviatoric stresses carried by the fine and coarse fractions for different values of fine content f_c at the initial, peak and critical states. The stress factors for the fine fraction are shown in Figure 13. It can be seen that at a low fine content ($f_c < 20\%$), the fine fraction carries almost zero-stress. This confirms that the fine particles are almost floating in voids between coarse particles. Skempton and Brogan [26] performed erosion tests on sandy gravels (binary mixtures of sands and gravels). The authors observed that some sandy gravels at low fine content are internally unstable, i.e. a significant proportion of sand content is washed out by water flow at low hydraulic gradient. The authors explained that, for these materials, a major part of the overburden load is carried by gravel particles, leaving the sand fraction under small stresses so sand particles can be easily washed out by water flow. The results shown above reinforce this explanation. It should be noted that a low stress carried by the fine fraction is just a necessary condition for the internal instability. This just means that fine particles can be easily detached by water flow. The sufficient condition is whether or not the primary fabric formed by solid particles allow detached fine particles to migrate within the interstices of this framework.

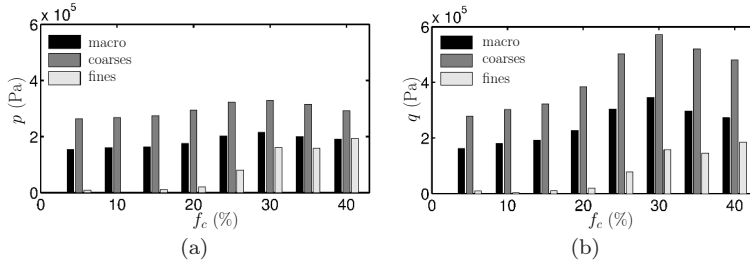


Fig. 12 The mean stress p (a) and the deviatoric stress q (b) carried by the fine and coarse fractions, compared to the macroscopic ones, versus fine content f_c at the peak state

At a higher fine content ($f_c \geq 20\%$), the fine particles participate in carrying the applied stress, and its participation increases with fine content. It is interesting to note that the fine fraction plays a more important role in carrying the mean stress than in carrying the deviatoric stress (Figure 13): at $f_c = 40\%$, $\alpha_p^F = 1.0$ compared to $\alpha_q^F = 0.6$ at the peak state. Shire et al. [24] also found that the stress factor α at the isotropic stress state increases with fine content; moreover it depends significantly on the particle size distribu-

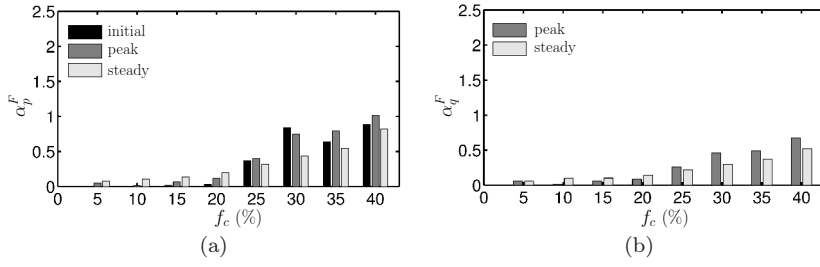


Fig. 13 Stress factors (a) α_p^F and (b) α_q^F defined for the fine fraction versus fine content f_c at the initial, peak and critical states.

tion curve. By investigating the stress factors α_p^F and α_q^F during a deviatoric loading, we find that the shearing leads to a significant reduction in the stress carried by the fine fraction (Figure 13). For $f_c = 30\%$, the stress factor α_p^F reduces indeed from 0.84 at the initial state to 0.43 at the critical state. It is worth noting that the sample with $f_c = 30\%$ exhibits the most marked softening behavior (Figure 4). This result indicates that the fine particles are unloaded during the softening phase, which might make them more vulnerable to internal erosion. Concerning the coarse fraction, since voids do not carry any stress and the fine fraction carries a stress smaller than the macroscopic stress, it carries a stress much bigger than the macroscopic stress. As shown in Figure 12, the stress carried by the coarse fraction is indeed about 1.6 times the macroscopic stress; moreover, it increases with fine content for $f_c \leq 30\%$ but decreases for $f_c > 30\%$ (Figure 12). This result confirms the optimal fine content $f_c = 30\%$ under which the coarse fraction is reinforced by fine particles and above which the coarse fraction is weakened since fine particles strongly separate them.

The partial stresses $\hat{\sigma}^F$ and $\hat{\sigma}^C$ defined in (5) give the contribution of each fraction to the macroscopic stress. If the solid fraction was homogeneous, the contribution of the fine fraction would be proportional to fine content f_c , e.g. 40% of fine content would contribute to 40% of the macroscopic stress. Figure 14 shows that the contribution of the fine fraction to the macroscopic stress is far from being proportional to fine content f_c . The fine particles do not significantly contribute to the macroscopic stress when $f_c < 20\%$ but they do when $f_c \geq 20\%$. A fine content of 40% contributes to 30.9% of the deviatoric stress q , but only 21.5% of the mean stress p at the peak state. It can be concluded that for the studied range of fine content, the coarse particles play a primary role in carrying the shear stress, while the fine particles play the role of a matrix that reinforces the coarse ones.

5 Classification of granular mixtures

According to Thevanayagam et al. [5], the micro-structure of granular mixtures can be constituted in many different ways, depending on fine content. The

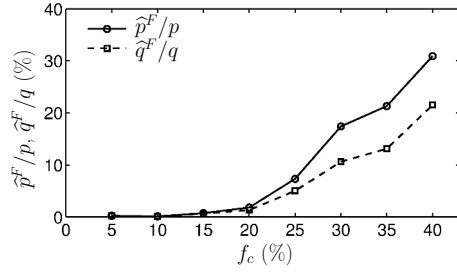


Fig. 14 Contributions of the fine fraction to the macroscopic mean and deviatoric stresses, p and q , at the peak state versus fine content f_c .

authors proposed three limiting categories of micro-structure: (a) the coarse-coarse contacts are dominant, (b) the fine-fine contacts are dominant, and (c) the fine and coarse particles form a layered system. The current study brought several interesting insights into the variation of the granular micro-structure and how the coarse-coarse, coarse-fine and fine-fine contacts participate in sustaining the shear stress, depending on fine content. It turns out that the fine-coarse contacts play an important role in the micro-structure and there exists an intermediate category between (a) and (b), where these contacts primarily bear the shear stress. We propose, therefore, the following classification of granular mixtures into four limiting categories of micro-structure with three threshold values as illustrated in Figure 15.

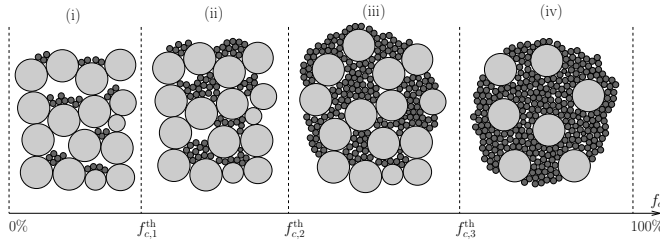


Fig. 15 Four categories of micro-structure for granular gap-graded soils

- Category (i) for $f_c < f_{c,1}^{\text{th}}$: the fine particles are almost floating within intercoarse voids, hence they have a little contribution to supporting the shear stress. The shear strength is then not affected by fine content.
- Category (ii) for $f_{c,1}^{\text{th}} \leq f_c < f_{c,2}^{\text{th}}$: the fine particles partially fill intercoarse voids but they partially separate coarse ones. The fine-coarse contacts are created and contribute to supporting the shear stress. However, contacts between coarse particles primarily carry the shear stress. In this case, the shear strength increases with fine content.
- Category (iii) for $f_{c,2}^{\text{th}} \leq f_c < f_{c,3}^{\text{th}}$: the fine particles fully fill intercoarse voids and greatly destroy coarse-coarse contacts. The fine-fine contacts

participate in carrying the shear stress. The role of the fine-coarse contacts becomes dominant. In this case, the shear strength decreases with fine content.

- Category (iv) for $f_c \geq f_{c,3}^{\text{th}}$: the coarse particles are fully dispersed by the fine ones. The behavior of granular mixtures of this category is mainly governed by the fine particles. It is thus expected that the shear strength is independent of fine content in this case.

It should be noted that this classification does not include the category (c) of layered micro-structure considered by Thevanayagam et al. For the binary mixtures considered in our study, the first and second threshold values, $f_{c,1}^{\text{th}}$ and $f_{c,2}^{\text{th}}$, are about 20% and 30%, respectively. We could not determine the third threshold value $f_{c,3}^{\text{th}}$ since the computation time for simulating binary mixtures with very high fine content is too long. It is worth mentioning that these threshold values might depend on many factors like the gap ratio, the particle shape or the sample density.

6 Conclusions

In this paper, we have presented a study on the effect of fine content on the mechanical behavior of granular gap-graded materials subjected to shear loading. Numerical samples composed of fine and coarse spherical particles with different values of fine content from 0% to 40% are simulated using the DEM. Triaxial compression tests are then performed on these samples and their behavior is investigated at the macro- and micro-scales. This study brought a lot of insights into the granular micro-structure of binary mixtures to explain why the fine particles can have no effect, positive effect or negative effect on their stress-strain behavior, depending on fine content. At a low fine content ($f_c < 20\%$), the fine particles are almost floating within the void space between the coarse particles so they do not participate significantly in carrying the shear stress. Starting from 20% of fine content, the fine particles cause two opposite effects to the granular micro-structure: on one hand, they come into contact with coarse particles and reinforce the micro-structure, but on the other hand, they separate coarse particles and then weaken the micro-structure. As a consequence, the shear stress is transmitted more and more through the coarse-fine contacts but less and less through the coarse-coarse contacts as fine content increases. The optimal fine content is about 30% under which the coarse-coarse contacts primarily support the shear stress. A decrease in the stress part carried by them is compensated by a strong increase in the stress part carried by the coarse-fine contacts. As a result, the shear strength increases with fine content. Above this optimal fine content, the coarse-fine contacts overtake the coarse-coarse contacts in carrying the shear stress. The network of the coarse-coarse contacts is greatly weakened and is not sufficiently reinforced by the coarse-fine and fine-fine contacts, hence the shear strength decreases. For the studied range of fine content, the fine-fine

contacts have little contribution to the macro-stress. It was also found that the strong force network at a high fine content, which is the skeleton to bear the external stress, includes almost all the coarse-coarse contacts but no more than 50% of coarse-fine contacts. Furthermore, a major fraction of fine-fine contacts are located in the weak force network.

For the studied range of fine content, the coarse particles constitute primarily the solid skeleton to resist to shear loading, leaving the fine particles under lower stresses. Interestingly, the role of the fine particles is more important in carrying the mean stress than in carrying the deviatoric stress. At a high fine content, the fine particles suffer a marked softening phase after the peak state.

Based on this study, a classification of binary mixtures into four limiting categories of micro-structure was proposed. The particularity of the proposed classification is that it considers the importance of the coarse-fine contacts in the micro-structure. When fine content exceeds a threshold value (about 30% in our simulations), these contacts overtake the coarse-coarse contacts in carrying the shear stress.

7 Acknowledgements

The authors would like to thank the charitable and cultural association of Nabatieh-Lebanon and Cedre program of the French and Lebanese scientific cooperation for the financial support for this research project.

References

1. Y.S. Sail, D. Marot, L. Sibille, and A. Alexis. Suffusion tests on cohesionless granular matter. *Eur. J. Environ. Civ. Eng.*, 15(5):799–817, 2011.
2. L. Ke and A. Takahashi. Strength reduction of cohesionless soil due to internal erosion induced by one-dimensional upward seepage flow. *Soils and Foundations*, 52(4):698–711, 2012.
3. L. Ke and A. Takahashi. Triaxial erosion test for evaluation of mechanical consequences of internal erosion. *Geotech. Test. J.*, 37(2), 2014.
4. R. Salgado, P. Bandini, and A. Karim. Shear strength and stiffness of silty sand. *J. Geotech. Geoenviron. Eng.*, 126(5):451–462, 2000.
5. S. Thevanayagam, T. Shenthan, S. Mohan, and J. Liang. Undrained Fragility of Clean Sands, Silty Sands, and Sandy Silts. *J. Geotech. Geoenviron. Eng.*, 128(10):849–859, 2002.
6. T.G. Murthy, D. Loukidis, J.A.H. Carraro, M. Prezzi, and R. Salgado. Undrained monotonic response of clean and silty sands. *Géotechnique*, 57(3):273–288, 2007.
7. T.-K. Nguyen, N. Benahmed, P.-Y. Hicher, and M. Nicolas. The influence of fines content on the onset of instability and critical state line of silty sand. In K.-T. Chau and J. Zhao, editors, *Bifurcation and Degradation of Geomaterials in the New Millennium*, pages 113–120. 2015.
8. F.H. Kim, D. Penumadu, J. Gregor, N. Kardjilov, and I. Manke. High-resolution neutron and X-ray imaging of granular materials. *J. Geotech. Geoenviron. Eng.*, 139(5):715–723, 2012.
9. N. Belheine, J.P. Plassiard, F.V. Donzé, F. Darve, and A. Seridi. Numerical simulation of drained triaxial test using 3D discrete element modeling. *Computers and Geotechnics*, 36(1):320–331, 2009.

10. N.H. Minh, Y.P. Cheng, and C. Thornton. Strong force networks in granular mixtures. *Granular Matter*, 16(1):69–78, 2014.
11. N.H. Minh and Y.P. Cheng. On the contact force distributions of granular mixtures under 1D-compression. *Granular Matter*, 18(2):1–12, 2016.
12. T. Shire and C. O’Sullivan. Micromechanical assessment of an internal stability criterion. *Acta Geotechnica*, 8(1):81–90, 2013.
13. T. Shire, C. O’Sullivan, and K.J. Hanley. The influence of fines content and size-ratio on the micro-scale properties of dense bimodal materials. *Granular Matter*, 18(3):1–10, 2016.
14. T.-T. Ng, W. Zhou, and X.-L. Chang. Effect of particle shape and fine content on the behavior of binary mixture. *J. Eng. Mech.*, 143(1):C4016008, 2016.
15. S. Luding. Introduction to discrete element methods: basic of contact force models and how to perform the micro-macro transition to continuum theory. *Eur. J. Environ. Civ. Eng.*, 12(7-8):785–826, 2008.
16. F. Radjai and V. Richefeu. Contact dynamics as a nonsmooth discrete element method. *Mechanics of Materials*, 41(6):715–728, 2009.
17. Šmilauer et al. Yade Documentation 2nd ed. *The Yade Project. DOI 10.5281/zenodo.34073* (<http://yade-dem.org/doc/>), 2015.
18. L. Scholtès, P.-Y. Hicher, and L. Sibille. Multiscale approaches to describe mechanical responses induced by particle removal in granular materials. *Comptes Rendus Mécanique*, 338(10-11):627–638, 2010.
19. D.S. Chang and L.M. Zhang. Extended internal stability criteria for soils under seepage. *Soils and Foundations*, 53(4):569–583, 2013.
20. D4767-88. Standard test method for consolidated-undrained triaxial compression test on cohesive soils. *Standard ASTM*, 04.08, 1988.
21. NF P 94-074. Sols: reconnaissances et essais – Essais à l’appareil triaxial de révolution. *AFNOR*, 1994.
22. J. Wiącek and M. Molenda. Representative elementary volume analysis of polydisperse granular packings using discrete element method. *Particuology*, 27:88 – 94, 2016.
23. C. Salot, P. Gotteland, and P. Villard. Influence of relative density on granular materials behavior: DEM simulations of triaxial tests. *Granular matter*, 11(4):221–236, 2009.
24. T. Shire, C. O’Sullivan, K.J. Hanley, and R.J. Fannin. Fabric and effective stress distribution in internally unstable soils. *J. Geotech. Geoenviron. Eng.*, 140(12):04014072, 2014.
25. B. Chareyre. *Modélisation du comportement d’ouvrages composites sol-géosynthétique par éléments discrets: application aux ancrages en tranchées en tête de talus*. PhD thesis, Université Grenoble I - Joseph Fourier, 2003.
26. A.W. Skempton and J.M. Brogan. Experiments on piping in sandy gravels. *Géotechnique*, 44(3):449–460, 1994.
27. S. Thevanayagam and S. Mohan. Intergranular state variables and stress-strain behaviour of silty sands. *Géotechnique*, 50(1):1–23, 2000.
28. P.V. Lade, C.D. Liggio, and J.A. Yamamuro. Effects of non-plastic fines on minimum and maximum void ratios of sand. *Geotech. Test. J.*, 21(4):336–347, 1998.
29. N.H. Minh and Y.P. Cheng. A DEM investigation of the effect of particle-size distribution on one-dimensional compression. *Géotechnique*, 63:44–53, 2013.
30. T. Shire, C. O’Sullivan, and K. Hanley. The influence of finer fraction and size-ratio on the micro-scale properties of dense bimodal materials. In K. Soga, K. Kumar, G. Biscontin, and M. Kuo, editors, *Geomechanics from Micro to Macro*, pages 231–236. 2014.
31. C. Thornton. Force transmission in granular media. *KONA Powder and Particle Journal*, 15:81–90, 1997.
32. F. Radjai and D.E. Wolf. Features of static pressure in dense granular media. *Granular Matter*, 1(1):3–8, 1998.
33. J.J. Christoffersen, M.M. Mehrabadi, and S.S. Nemat-Nasser. A micromechanical description of granular material behavior. *J. Appl. Mech.*, 48(2):339–344, 1981.
34. J.J. Moreau. Numerical investigation of shear zones in granular materials. In *Friction, Arching, Contact Dynamics*, pages 233–247. World Scientific, Singapore, 1997.
35. L. Staron, F. Radjai, and J.P. Vilotte. Multi-scale analysis of the stress state in a granular slope in transition to failure. *Eur. Phys. J. E: Soft Matter and Biol. Phys.*, 18(3):311–320, 2005.